Tribology International 131 (2019) 672–678

Contents lists available at ScienceDirect

Tribology International

journal homepage: www.elsevier.com/locate/triboint

Ti6Al4V-PEEK multi-material structures – design, fabrication and tribological characterization focused on orthopedic implants

F. Bartolomeu[a,*], C.S. Abreu[a,b], C.G. Moura[a], M.M. Costa[a], N. Alves[c], F.S. Silva[a], G. Miranda[a]

[a] Center for Micro-Electro Mechanical Systems (CMEMS-UMinho), University of Minho, Campus de Azurém, 4800-058, Guimarães, Portugal
[b] Physics Department, Porto Superior Engineering Institute, ISEP, Portugal
[c] Centre for Rapid and Sustainable Product Development Polytechnic Institute of Leiria, Rua General Norton de Matos, Apartado 4133, 2411-901, Leiria, Portugal

ARTICLE INFO

Keywords:
Ti6Al4V-PEEK
Selective laser melting
Multi-material design
Tribological characterization

ABSTRACT

A multi-material concept that gathers Ti6Al4V and PEEK properties in a cellular structured component was designed, fabricated and investigated targeting hip implants. SLM and pressure assisted injection techniques were used to obtain Ti6Al4V-PEEK multi-material structures. Aiming to reproduce to some extension the tribological phenomena occurring during and after hip implant insertion, five tribological tests were outlined and performed. The obtained results showed that the presence of PEEK on the Ti6Al4V-PEEK cellular structures led to a substantial improvement on the wear resistance (62% reduction in the mass loss) when compared to the material currently available on market for hip implants. The multi-material solution here investigated shows a good compromise between the primary stability after implant insertion and the wear performance.

1. Introduction

In recent years, Additive Manufacturing (AM) technologies became one of the hot topics of research and, also from an industrial point of view, AM is attracting an ever growing attention of the manufacturing industries worldwide [1]. AM fabrication processes offer significant benefits for widespread industries, positively influencing society, economy and environmental increasing awareness in production sustainability. When using AM fabrication methods, a physical part is directly and easily obtained from a CAD data [2,3]. This aspect triggers a revolutionary capability to produce highly complex and customized products with no extra costs usually associated to extra tools, or molds that arise on conventional processing routes as casting e.g. Refs. [4–7]. Selective Laser Melting (SLM) is an AM technique that allows the construction of 3D components [8,9] by a cyclic process, allowing to fabricate a product layer-by-layer using laser energy to melt powder beds. As a layer-wise technique, SLM versatility allows the production of customized products with complex geometries such as cellular structures [10,11].

Ti6Al4V is the most widely used titanium alloy and it is one of the most used materials on SLM, especially because its properties fit several requirements for numerous industries [12]. Ti6Al4V products can be found in a widespread range of high-added-value components such as aerospace and aeronautics, transports and automotive and medicine [13–16]. High strength, relatives low weight and low elastic modulus, biological compatibility and higher corrosion resistance [17–19] can be pointed as the main properties of Ti6Al4V alloy. Nevertheless, Ti6Al4V displays a modest wear performance which plays a crucial role in biomedical applications where relative motion occurs between parts in orthopedic applications such as hip implants [20,21].

Even considering the great advances that have been achieved in the biomedical field, corrosion and wear are still recognized to lead to failure [22–26]. The wear debris lead to severe adverse responses and can require revision surgery. In fact, unsuited stiffness, fatigue strength, corrosion and wear resistance are pointed as the key issues that define the longevity of endosseous implants [25,27,28]. Despite, the ability of Ti6Al4V to form a very stable passive layer covering its surface, in the potentially corrosive environment of human body, a poor wear resistance can accelerate corrosion and lead to the inability in forming a very stable passive layer [20,29].

Dense Ti6Al4V is still being extensively used as hip implant material, however, stiffness mismatch and wear performance are still being pointed as critical causes to implant failure [30–33]. In order to enhance Ti6Al4V implants longevity, numerous studies have been carried out regarding coatings, surface treatments, functionally graded materials, porous and composite materials [34–37]. Poly-ether-ether-ketone (PEEK) is a polymer with high chemical stability, wear and corrosion resistance. However, PEEK cannot be used as implant material due to its low mechanical strength and elastic modulus (~ 3 GPa) when compared to cortical human bone (~ 20 GPa).

* Corresponding author.
E-mail address: flaviojorgebartolomeu@gmail.com (F. Bartolomeu).

https://doi.org/10.1016/j.triboint.2018.11.017
Received 30 August 2018; Received in revised form 27 September 2018; Accepted 15 November 2018
Available online 20 November 2018
0301-679X/

PEEK either in its natural form or reinforced has been used as arthroplasty bearing material for several applications such finger joints, acetabular cups, tibial inserts [38]. When thinking about hip implants, typically made of Ti6Al4V, a possible solution could be to combine this metal with PEEK, via a structured design, to help overcome some of its shortcomings like the tribological and tribocorrosion performance [39]. For this purpose, it is important to understand the biological response to PEEK and to the generated wear debris once it can lead to implant loosening. Ashley A. Stratton-Powell et al. [40] prepared a systematic review to understand the biologic response of PEEK-based wear debris released from total joint arthroplasties. The wear particles produced by PEEK-based bearings were, in almost all cases, in the phagocytozable size range (0.1–10 μm). According to this review the biologic response to PEEK-based particles is generally found having cytotoxicity within acceptable limits.

This study proposes a smart design of a multi-material Ti6Al4V-PEEK component, that gathers Ti6Al4V and PEEK properties allowing to lower the stiffness mismatch between the implant material and bone, also to improve expressively the wear performance compared to fully dense metals currently used in hip implants.

2. Experimental details

2.1. Materials

Ti6Al4V powder from *SLM Solutions* (Germany) with a D90 of 40 μm and a D50 of 34 μm was used to produce dense and cellular Ti6Al4V structures by using Selective Laser Melting technique. PEEK powder purchased from *Evonik Industries* (Germany) was also used to fabricate Ti6Al4V-PEEK specimens. Fig. 1 depicts SEM images of Ti6Al4V and PEEK powders. Additionally, commercial Ti6Al4V cast/forged alloy bar purchased from *Titanium Products Ltd.* (United Kingdom) was used as a control specimen, representing the current titanium alloy used on orthopedic applications.

2.2. Design and fabrication details

In the present study, four groups of Ti6Al4V specimens (cylinders with 6 mm diameter and 3 mm of thickness) were investigated as can be seen inTable 1. G1 (Cast/Forged) was obtained from a Ti6Al4V bar. G2, G3 and G4 Ti6Al4V specimens were fabricated by using a Selective Laser Melting equipment (model 125HL) from *SLM Solutions*. CAD software was used to prepare dense (G2) and cellular structured (G3 and G4) cylindrical specimens. Later, these data were incorporated into SLM software and finally the specimens were fabricated.

The SLM fabrication of G2, G3 and G4 was carried out operating with the following processing parameters: 90 W for the laser power, scan speed of 600 mm/s, 80 μm of scan spacing and 30 μm of layer thickness. These groups were modeled by using CAD software in which cubic-like structures were designed with open-cells of 450 μm and walls thickness of 350 μm. The aforementioned processing parameters were defined based on a prior optimization study [12].

Table 1
Ti6Al4V-based specimens fabrication strategy, materials and structure.

	Fabrication strategy	Materials and structure
G1	Cast/Forged	Ti6Al4V Dense
G2	Selective Laser Melting	Ti6Al4V Dense
G3	Selective Laser Melting	Ti6Al4V cellular structured
G4	Selective Laser Melting and Pressure assisted injection	Ti6Al4V cellular structured and PEEK

After SLM production, some Ti6Al4V specimens were used to produce the multi-material specimens (referred in this study as G4). For that purpose and by means of Pressure assisted injection, PEEK was forced to fill the open-cells of the cellular structured specimens. In pressure assisted injection technique, pressure and temperature are simultaneously applied. Firstly, a Ti6Al4V cellular specimen is positioned inside a mold and secondly PEEK powder is introduced. Afterwards, the top punch is inserted in the mold and the system is placed inside a chamber with a vacuum atmosphere of 10^2 mbar. An initial residual pressure is applied in order to accommodate the PEEK powder and then the induction heating starts till 380 °C (above the melting point of PEEK (345 °C)). After this, the temperature is decreased until 300 °C and a pressure of 25 MPa is applied for 5 s. Finally, the multi-material Ti6Al4V-PEEK structure is removed from the mold. A schematic representation of the injection route used is illustrated in Fig. 2.

2.3. Surface preparation and roughness measurements

The specimens were subjected to a surface treatment in order to obtain a moderate surface roughness, R_a, around 2 μm, similar to the finishing found in commercial implants. The surfaces of the specimens were sandblasted with spherical alumina particles (average diameter of 149 μm, according to the manufacturer – Blasquem - Portugal) during 30 s and then cleaned in an ultrasonic bath immersed in isopropyl alcohol for 5 min. After preparation, the surface roughness was assessed by means of a surface profilometer (Surftest SJ 201, Mitutoyo). The surface roughness measurements were performed according to the ISO 4287-1997 standard, with an evaluation length of 3 mm, a cutoff wavelength of 0.8 mm and scan speed of 0.25 mm/s. At least 4 measurements were performed for each specimen.

2.4. Ti6Al4V–alumina tribological interaction

In this study, an alumina (Al_2O_3) plate with $4 \times 12 \times 2\ mm^3$ was used as reference antagonistic material to perform sliding tests against G1, G2, G3 and G4 specimens. The tribological performance of the produced Ti6Al4V-based specimens against the alumina plate was assessed by using a *Bruker-UMT-2* (USA) tribometer. Fig. 3 aims to show

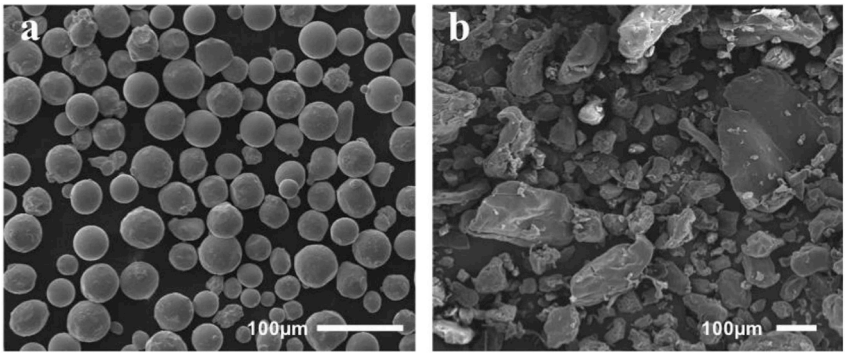

Fig. 1. SEM images of (a) Ti6Al4V and (b) PEEK powders.

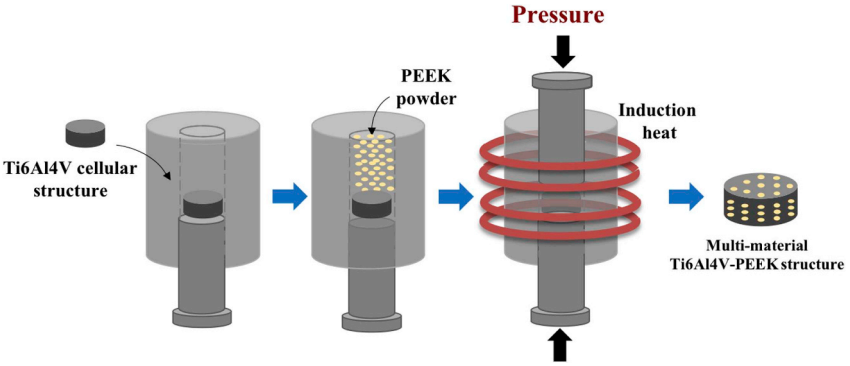

Fig. 2. Pressure assisted injection procedure to introduce PEEK into the Ti6Al4V cellular structures.

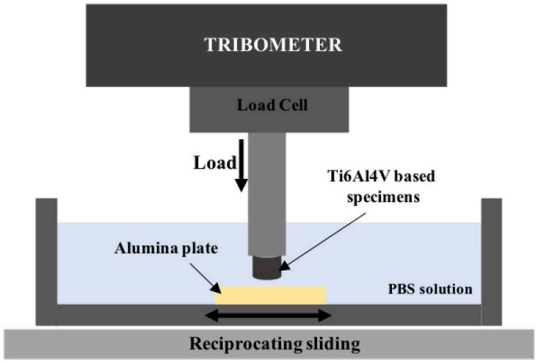

Fig. 3. Schematic representation of the tribological test.

schematically the apparatus used to perform the tests. The Ti6Al4V-based specimens were placed on an upper metallic sample holder fixed to a load cell and the alumina plate was mounted on an acrylic die fixed to the tribometer's oscillatory table. All the tests were carried out immersed in a Phosphate Buffer Solution (PBS) medium.

Aiming to reproduce to some extension the tribological phenomena occurring during and after hip implant insertion, five tribological tests were outlined and performed. All of these tests used the following constant settings: 50 N for the applied load and a frequency of 1 Hz (approximating human gait). These five tests reasoning are as follows:

- In the begin of the implant insertion, hip implant is positioned and, firstly, at the implant surface level, there is an opposition of the bone to implant material movement, that can be appraised by the initial static coefficient of friction. For this assessment, a T1 test, named “Static initial”, was performed.
- When the surgeon inserts the implant into the bone cavity, an interaction between implant and bone will occur, being this aspect assessed in T2 test, named “Insertion test implantation. This interaction between implant material during its course in the bone cavity was assessed after the static initial test. A total sliding distance of 100 mm was defined in order to replicate the travel distance of a hip implant along the bone cavity during the implantation surgery [41].
- When the implant gets locked with a specific stability, a final assessment can be made, to evaluate the final friction coefficient (T3 test, named “Static final”). This final opposition dictates the finally stability of the implant being commonly referred in literature primary stability [17,42].
- Fretting experiments aiming to study the micro-movements (~100 μm) that occur between implant and bone after implantation were also performed (T4 tests, named “Fretting”).
- Finally, a conventional wear test was also performed for determining the wear performance of these materials against alumina. This was named “Tribological performance” test (T5).

Table 2
Testing parameters used on the performed tribological tests.

Test designation	Load (N)	Stroke length (mm)	Sliding distance (mm)	Frequency (Hz)
T1 - Static initial	50	–	–	–
T2 – Insertion test	50	5	100	1
T3 - Static final	50	–	–	–
T4 – Fretting	50	0.1	180	1
T5 – Tribological performance	50	5	18000	1

Table 2 summarizes the parameters of the five interaction tests performed in Ti6Al4V-based specimens against an alumina plate. For these tests, at least four specimens were tested per group.

2.5. Scanning electron microscopy (SEM) analysis

SEM analysis was used to characterize the morphology of the powders and of the Ti6Al4V-based specimens. SEM micrographs of Ti6Al4V-based structures after sandblasting (Fig. 4), following acid etching with Kroll's reagent (5% HNO_3, 10% HF and 85% of distilled water) (Fig. 6) and after the tribological tests (Fig. 8) are presented.

2.6. Statistical analysis

All the experimental results obtained in this study are described as the average value ± standard deviation. In order to investigate differences between groups, one-way ANOVA with post hoc Bonferroni's multiple comparison test was performed. Statistical significance was defined for $p < 0.05$ and GraphPad Prism v6 from GraphPad Software, (USA) was used.

3. Results and discussion

3.1. Morphology analysis and surface roughness

In this study, dense (G1 and G2) and cellular structured (G3 and G4) Ti6Al4V-based specimens were fabricated, sandblasted and tested. Fig. 4 shows the top surfaces of these specimens.

Regarding the dense specimens, Fig. 4 (a) and (b) show Ti6Al4V produced by cast/forging and SLM, respectively. A Ti6Al4V cellular structured specimen produced by SLM is shown in Fig. 4 (c), having the following experimentally measured dimensions: wall thickness of 454 μm and open-cell size of 336 μm. The differences detected between the CAD and the produced structures are typical on SLM fabrication process and are explained in literature [19,43]. Finally, Fig. 4 (d) shows the Ti6Al4V-PEEK multi-material specimen produced by SLM and pressure assisted injection.

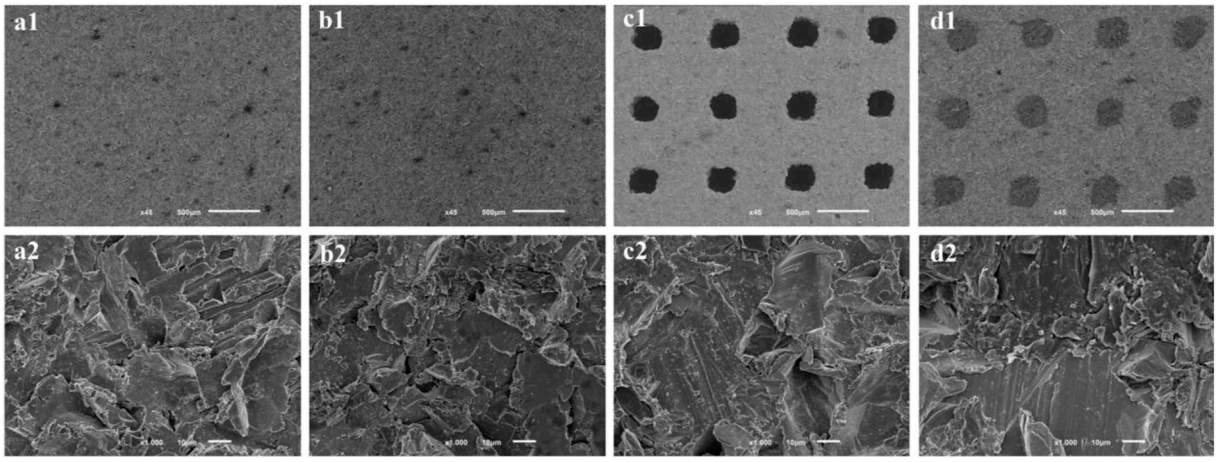

Fig. 4. Low and high magnification SEM images of Ti6Al4V-based specimen's surfaces after sandblasting: (a) G1, (b) G2, (c) G3 and (d) G4.

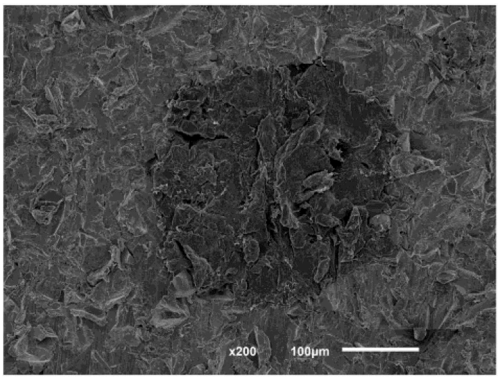

Fig. 5. SEM image of the top surface of the Ti6Al4V-PEEK interface present on the multi-material (G4) specimen.

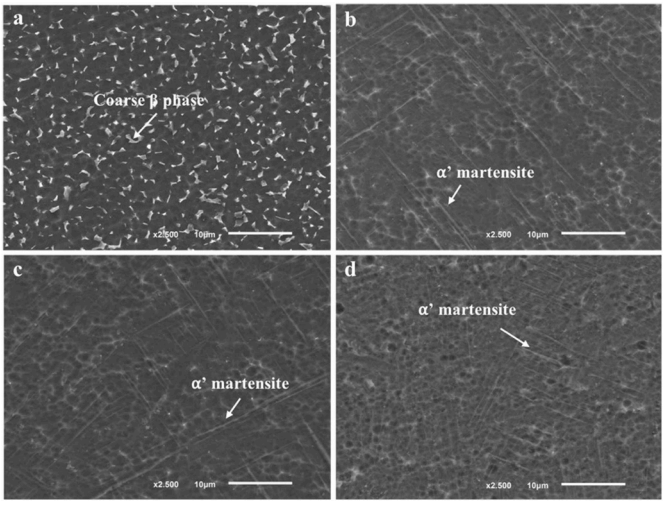

Fig. 6. SEM micrographs of the top surfaces of polished/acid-etched Ti6Al4V specimens: (a) G1; (b) G2; (c) G3 and (d) G4.

Fig. 5 depicts a detail SEM image of a Ti6Al4V-PEEK multi-material specimen (G4). This micrograph allows to observe the interface between the polymer and the metallic structure, validating the impregnation process and proving that an effective mechanical interlocking between PEEK and the Ti6Al4V structure was achieved.

Prior to the tribological tests, the surface roughness of all the specimens was characterized by means of a surface profilometer. The average values obtained for the surface roughness (Ra), the root mean square (Rq) and the maximum height of the profile (Rz) are presented in Table 3.

By analyzing Fig. 4 and Table 3, it can be seen that G1, G2, G3 and

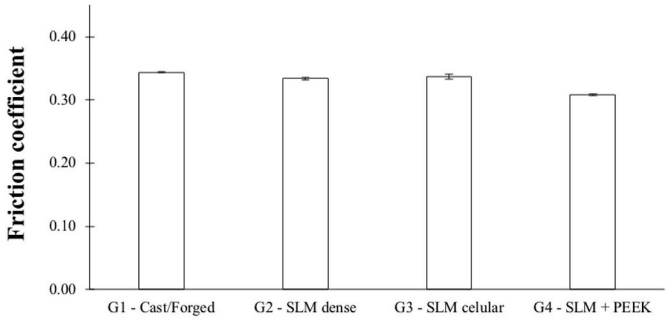

Fig. 7. Friction coefficient values obtained for T5 (Tribological performance).

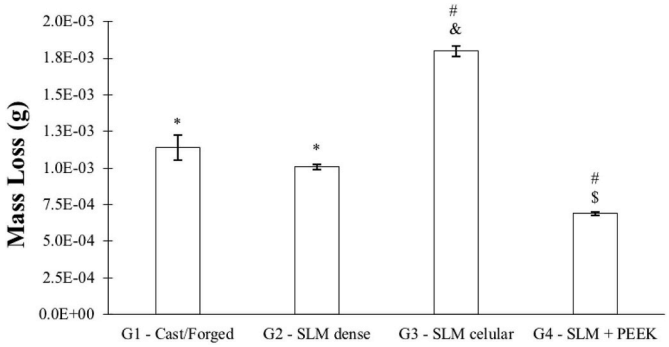

Fig. 8. Mass loss results obtained from test T5 of Ti6Al4V-based specimens G1, G2, G3 and G4 against an alumina plate under a normal load of 50 N, frequency of 1 Hz and 5 mm of stroke length in PBS. Symbols denote statistically significant differences ($p < 0.05$) in comparison to: (*) G3 and G4; (#) G1 and G2; ($) G3 and (&) G4.

Table 3
Surface roughness parameters (Ra, Rq and Rz) of Ti6Al4V-based specimen's top surface.

	R_a [μm]	R_q [μm]	R_z [μm]
G1	2.32 ± 0.07	2.98 ± 0.12	20.62 ± 0.08
G2	2.69 ± 0.08	3.45 ± 0.09	22.51 ± 1.00
G3	2.17 ± 0.15	3.04 ± 0.07	17.07 ± 2.52
G4	2.15 ± 0.20	3.04 ± 0.26	26.56 ± 1.93

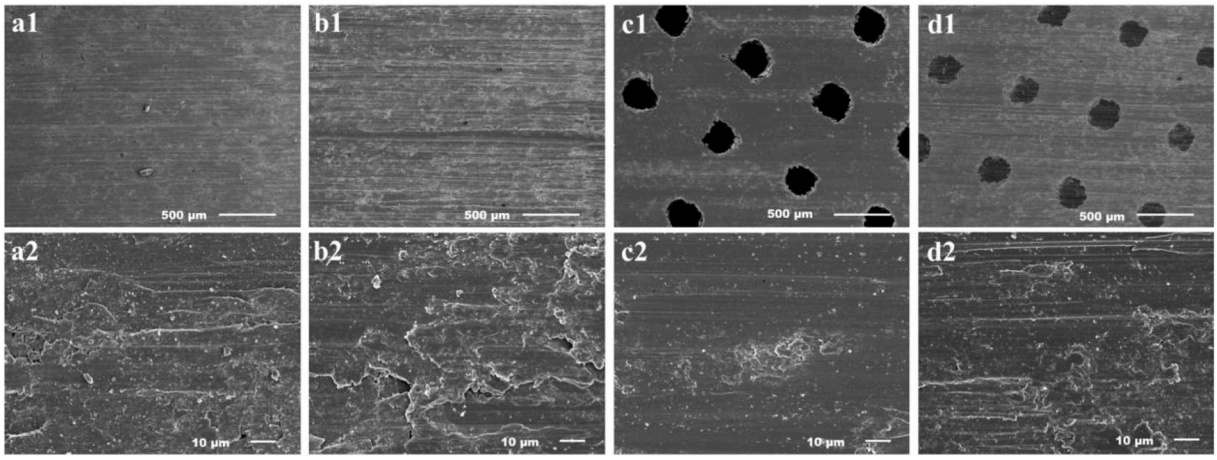

Fig. 9. SEM images of Ti6Al4V-based specimens worn surfaces: (a) G1, (b) G2, (c) G3 and (d) G4.

G4 specimens exhibit similar rough surfaces with macro and microscale morphology features. At the macroscale level predominant features are associated to the surface irregularities with a size range of 17.07–26.56 μm (Rz), while at the microscale, features with average dimensions in the leeway 2.15–2.69 μm (Ra) are found. Several studies have been reported in which a moderate surface roughness (Ra from 2 to 4 μm) enhances the implant osteointegration, therefore accelerating bone-biomaterial biological interaction [25,44,45]. In fact, the surface preparation used in this study allowed to obtain surfaces with a roughness similar to that used by implants manufacturers such as Straumann, Bego and Ankylos [19].

In this study, several processing routes were used, solely or combined, to produced Ti6Al4V-based specimens, viz. cast/forging, Selective Laser Melting and Pressure assisted injection. The specific characteristics of each processing route can dictate different microstructural features of Ti6Al4V alloy, whose microstructure is decidedly associated with the cooling rate induced by the processing route from above β transus temperature [46,47].

Ti6Al4V components fabricated by means of cast/forging usually display a α–β coarse structure, as can be seen on Fig. 6 (a), once the material experiences a slow to intermediate cooling rate during processing [48,49]. Contrarily, the SLM process induces extremely fast cooling rates (10^3–10^6 K/s), leading to microstructures with an acicular morphology resulting from the transformation of β-phase to martensitic α′-phase. In fact, the acicular morphology is present on Fig. 6 (b, c and d), therefore validating the typical structure obtained when using SLM. The pressure assisted injection technique used to introduce PEEK into the open-cells of the Ti6Al4V cellular structures do not lead to visible microstructural differences, due to the low temperature used (380 °C).

3.2. Tribological behavior

Fig. 7 shows the friction coefficient values obtained on the tribological test T5 (Tribological performance).

When analyzing the results obtained for T5 tests (Tribological performance), a slightly lower (10%) friction coefficient is displayed by G4 (multi-material Ti6Al4V-PEEK structures) when compared to G1 cast/forged specimens. This slightly decrease on the friction coefficient can be explained by the self-lubrication ability of PEEK, as reported by other authors [50].

Fig. 8 depicts the mass loss values for all the Ti6Al4V-based specimens studied, sliding against an alumina plate under 50 N of applied load and distance of 18 m.

Taking into consideration Fig. 8, significant differences on mass loss between the different groups were observed. Ti6Al4V cellular structures (G3) exhibited the worst wear resistance with, therefore, the highest value for mass loss (1.80 mg). In G3 specimens, for a same applied load, the presence of open-cells (i.e. empty regions) lead to higher contact pressures in regions with material, when compared to the other groups, which aggravates the contact damage against the hard Al_2O_3 ceramic and, therefore, increases wear loss.

When comparing G1 (current material used in orthopedic applications) and G2 systems some differences arise. G2 displayed a slightly (11%) higher wear resistance, when compared to G1. This difference can be explained based on the microstructural differences described in Fig. 6, since the presence of α′ martensite phase has been reported to increase the strength and hardness of Ti6Al4V alloy produced by SLM, when compared to cast/forging processing route [12]. Thus, the higher hardness lead to increased wear resistance of G2 according to Archard's wear equation [3,51].

The multi-material Ti6Al4V-PEEK cellular structure showed the best wear resistance with an average mass loss of 0.690 mg. When comparing the two cellular structures results (G3 and G4) a higher wear resistance was found for G4, with a 62% reduction in the mass loss of this group. Moreover, when comparing G4 with the commercial similar system G1 (similar to commercial solution) a 40% decrease in mass loss can be noted for the former.

The superior wear resistance of PEEK, that is filling the open-cells as well as its auto-lubrication properties, are accountable for lowering meaningfully the mass loss in G4 specimens [18,20,50]. In addition, these results prove that the developed multi-material Ti6Al4V-PEEK solution displays a superior performance when compared to the current available commercial titanium implants (e.g. hip implants and tibial plates).

Fig. 9 shows SEM images of all the specimens after tribological interaction, where the damage features linked to the prevailing wear mechanisms that take place during the sliding against alumina plate are visible. Evidences of plastic deformation of the wear debris and subsequent clustering to form tribolayers as well as abrasive grooves parallel to the sliding direction can be seen, in more or less proportions, for all systems. These abrasion grooves are generated by protruding alumina hard asperities, resulting in a two bodyabrasive wear mode leading to the surface damage and loss of material in Ti6Al4V-based specimens. Besides, a fine scale polishing wear mechanism can be observed in the worn surfaces of all the studied systems.

Additionally, the wear tracks on the alumina plate resulting from the tribotests carried out against all studied Ti6Al4V-based systems were analyzed by SEM and EDS. Chemical analysis of the wear debris adhered to the antagonistic surface showed the presence of Ti, Al and V elements, which confirms the transfer of material as a result of wear of the softer Ti6Al4V-based material to the ceramic by a combination of adhesion and mechanical interlocking resulting from the surface

Table 4
Friction coefficient (average ± standard deviation) obtained in T1 (Static initial) and T3 (Static final) tests.

	Static initial	Static final
G1 – Cast/Forged	0.394 ± 0.001	0.393 ± 0.024
G2 – SLM dense	0.382 ± 0.011	0.418 ± 0.032
G3 – SLM cellular	0.402 ± 0.014	0.410 ± 0.004
G4 – SLM + PEEK	0.377 ± 0.001	0.359 ± 0.002

roughness. In the case of the wear tracks created due to the sliding tests of G4, PEEK also adhered to the alumina plate.

Table 4 and Fig. 10 present the results obtained for the static, dynamic and fretting sliding tests performed in this study.

As mentioned above, when an implant is firstly positioned, there is an opposition to the implant movement due to friction with the bone.

The T1 test ("Static initial") was performed to characterize this stage. When the implant reaches the end of the insertion cavity and becomes attached with a specific stability, a final friction coefficient can be analyzed (from T3 test - "Static final"), that correlates with the implant stability after insertion [17,42].

Looking at the results of Table 4, no significant differences were observed between G1, G2 and G3, as for the static initial COF as well as for the static final friction, with both exhibiting values around 0.40. The G4 multi-material Ti6Al4V-PEEK structures exhibit a slightly lower COF, either for static initial and static final assessments when compared to G1, once more due to the presence of PEEK and its self-lubricating effect.

The interaction between the implant material during its course in the bone cavity was assessed by performing T2 test - "Insertion test". When looking at the results obtained for the T2 test (Fig. 10) similar average COF values were obtained for all the groups tested. Contrarily, to T5 tests, where some differences on the COF are noticed between G4 and the other systems, for this static initial test no differences are perceived.

Fretting experiments (stroke length of ~100 μm) performed to replicate the micromotions between implant and bone after implantation (T4 tests - "Fretting") allowed to conclude that no significant differences exist among the various groups. A friction coefficient around 0.1 is reported in literature for dense PEEK [38]. In this sense, it would be expectable to find a lower friction coefficient in the case of G4 (Ti6Al4V-PEEK structures) for T4 tests, however these were found similar to the other groups. In fact, previously, M. Buciumeanu et al. [20] reported no significant different on the friction coefficient between Ti6Al4V and Ti6Al4V-PEEK cellular structures with different open-cells size when tested against alumina. In this sense, the similarity on the friction coefficient among these various groups can be explained based on the formation of a metallic (Ti6Al4V) tribolayer that controls the sliding and then the friction coefficient.

The obtained results showed that the presence of PEEK on the Ti6Al4V-PEEK cellular structures led to a slightly decrease on the friction coefficient (Figs. 7 and 10) and led to a substantial improvement on the wear resistance when compared to the G1 system, which represents the material currently available on market for hip implants. The multi-material Ti6Al4V-PEEK solution here investigated proposes a good compromise between the primary stability (immediately after implant insertion) and the wear performance.

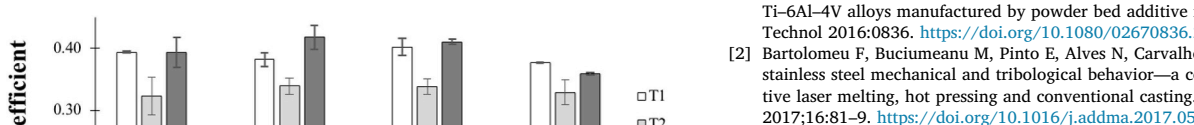

Fig. 10. Friction coefficient values obtained for T1 (Static initial), T2 (Insertion test), T3 (Static final) and T4 (Fretting) tests.

4. Conclusions

The following detailed conclusions can be drawn from this work:

- Selective Laser Melting technique was used to fabricate cubic-shaped Ti6Al4V cellular structures with wall thickness of 454 μm and open-cells size of 336 μm;
- Pressures assisted injection was successfully used to introduce PEEK in the structure's open-cells aiming to obtain multi-material Ti6Al4V-PEEK cellular structures;
- The Ti6Al4V-PEEK multi-material structures displayed an enhanced wear performance due to the auto-lubrication properties of PEEK;
- The Ti6Al4V-PEEK multi-material structures improved wear performance was characterized, by a 40% lower mass loss compared to conventional cast/forged materials used in implants, and 62% lower mass loss compared to Ti6Al4V cellular structures.

Cofinanciado por:
COMPETE 2020
PORTUGAL 2020
UNIÃO EUROPEIA
Fundo Europeu de Desenvolvimento Regional
FCT
Fundação para a Ciência e a Tecnologia
MINISTÉRIO DA EDUCAÇÃO E CIÊNCIA

Image 2

Acknowledgements

This work was supported by FCT through the grants SFRH/BD/128657/2017 and SFRH/BPD/112111/2015, the project PTDC/EMS-TEC/5422/2014 and also by project NORTE 01-0145_FEDER-000018. Additionally, this work was supported by FCT with the reference project UID/EEA/04436/2013, by FEDER funds through the COMPETE 2020 – Programa Operacional Competitividade e Internacionalização (POCI) with the reference project POCI-01-0145-FEDER-006941.

References

[1] Tong J, Bowen CR, Persson J, Plummer A. Mechanical properties of titanium-based Ti–6Al–4V alloys manufactured by powder bed additive manufacture. Mater Sci Technol 2016:0836. https://doi.org/10.1080/02670836.2016.1172787.
[2] Bartolomeu F, Buciumeanu M, Pinto E, Alves N, Carvalho O, Silva FS, et al. 316L stainless steel mechanical and tribological behavior—a comparison between selective laser melting, hot pressing and conventional casting. Addit Manuf 2017;16:81–9. https://doi.org/10.1016/j.addma.2017.05.007.
[3] Bartolomeu F, Buciumeanu M, Pinto E, Alves N, Silva FS, Carvalho O, et al. Wear behavior of Ti6Al4V biomedical alloys processed by selective laser melting, hot pressing and conventional casting. Trans Nonferrous Met Soc China (English Ed) 2017;27:829–38. https://doi.org/10.1016/S1003-6326(17)60060-8.
[4] Bordin A, Sartori S, Bruschi S, Ghiotti A. Experimental investigation on the feasibility of dry and cryogenic machining as sustainable strategies when turning Ti6Al4V produced by Additive Manufacturing. J Clean Prod 2016;142:4142–51. https://doi.org/10.1016/j.jclepro.2016.09.209.
[5] Nicoletto G. Anisotropic high cycle fatigue behavior of Ti-6Al-4V obtained by powder bed laser fusion. Int J Fatig 2016;94:255–62. https://doi.org/10.1016/j.ijfatigue.2016.04.032.
[6] Van Hooreweder B, Apers Y, Lietaert K, Kruth JP. Improving the fatigue

performance of porous metallic biomaterials produced by Selective Laser Melting. Acta Biomater 2017;47:193–202. https://doi.org/10.1016/j.actbio.2016.10.005.
[7] Dallago M, Fontanari V, Torresani E, Leoni M, Pederzolli C, Potrich C, et al. Fatigue and biological properties of Ti-6Al-4V ELI cellular structures with variously arranged cubic cells made by selective laser melting. J Mech Behav Biomed Mater 2018;78:381–94. https://doi.org/10.1016/j.jmbbm.2017.11.044.
[8] Miranda G, Faria S, Bartolomeu F, Pinto E, Madeira S, Mateus A, et al. Materials Science & Engineering A Predictive models for physical and mechanical properties of 316L stainless steel produced by selective laser melting. Mater Sci Eng, A 2016;657:43–56. https://doi.org/10.1016/j.msea.2016.01.028.
[9] Bose S, Ke D, Sahasrabudhe H, Bandyopadhyay A. Additive manufacturing of biomaterials. Prog Mater Sci 2018;93:45–111. https://doi.org/10.1016/j.pmatsci.2017.08.003.
[10] Xu Y, Zhang D, Zhou Y, Wang W, Cao X. Study on topology optimization design, manufacturability, and performance evaluation of Ti-6Al-4V porous structures fabricated by selective laser melting (SLM). Materials (Basel) 2017;10. https://doi.org/10.3390/ma10091048.
[11] Zhou B, Zhou J, Li H, Lin F. A study of the microstructures and mechanical properties of Ti6Al4V fabricated by SLM under vacuum. Mater Sci Eng, A 2018;724:1–10. https://doi.org/10.1016/j.msea.2018.03.021.
[12] Bartolomeu F, Faria S, Carvalho O, Pinto E, Alves N, Silva FS, et al. Predictive models for physical and mechanical properties of Ti6Al4V produced by Selective Laser Melting. Mater Sci Eng, A 2016;663:181–92. https://doi.org/10.1016/j.msea.2016.03.113.
[13] Ellyson B, Chekir N, Brochu M, Brochu M. Characterization of bending vibration fatigue of WBD fabricated Ti-6Al-4V. Int J Fatig 2017;101:36–44. https://doi.org/10.1016/j.ijfatigue.2017.03.045.
[14] Li W, Yan L, Karnati S, Liou F, Newkirk J, Taminger KMB, et al. Ti-Fe intermetallics analysis and control in joining titanium alloy and stainless steel by Laser Metal Deposition. J Mater Process Technol 2017;242:39–48. https://doi.org/10.1016/j.jmatprotec.2016.11.010.
[15] Taniguchi N, Fujibayashi S, Takemoto M, Sasaki K, Otsuki B, Nakamura T, et al. Effect of pore size on bone ingrowth into porous titanium implants fabricated by additive manufacturing: an in vivo experiment. Mater Sci Eng C 2016;59:690–701. https://doi.org/10.1016/j.msec.2015.10.069.
[16] Mahtabi MJ, Shamsaei N, Mitchell MR. Fatigue of Nitinol: the state-of-the-art and ongoing challenges. J Mech Behav Biomed Mater 2015;50:228–54. https://doi.org/10.1016/j.jmbbm.2015.06.010.
[17] Dantas TA, Abreu CS, Costa MM, Miranda G, Silva FS, Dourado N, et al. Bioactive materials driven primary stability on titanium biocomposites. Mater Sci Eng C 2017;77:1104–10. https://doi.org/10.1016/j.msec.2017.04.014.
[18] Sampaio M, Buciumeanu M, Henriques B, Silva FS, Souza JCM, Gomes JR. Tribocorrosion behavior of veneering biomedical PEEK to Ti6Al4V structures. J Mech Behav Biomed Mater 2016;54:123–30. https://doi.org/10.1016/j.jmbbm.2015.09.010.
[19] Bartolomeu F, Sampaio M, Carvalho O, Pinto E, Alves N, Gomes JR, et al. Tribological behavior of Ti6Al4V cellular structures produced by Selective Laser Melting. J Mech Behav Biomed Mater 2017;69:128–34. https://doi.org/10.1016/j.jmbbm.2017.01.004.
[20] Buciumeanu M, Almeida S, Bartolomeu F, Costa MM, Alves N, Silva FS, et al. Ti6Al4V cellular structures impregnated with biomedical PEEK - new material design for improved tribological behavior. Tribol Int 2018;119:157–64. https://doi.org/10.1016/j.triboint.2017.10.038.
[21] Toptan F, Rego A, Alves AC, Guedes A. Corrosion and tribocorrosion behavior of Ti-B4C composite intended for orthopaedic implants. J Mech Behav Biomed Mater 2016;61:152–63. https://doi.org/10.1016/j.jmbbm.2016.01.024.
[22] Rodrigues DC, Valderrama P, Wilson TG, Palmer K, Thomas A, Sridhar S, et al. Titanium corrosion mechanisms in the oral environment: a retrieval study. Materials (Basel) 2013;6:5258–74. https://doi.org/10.3390/ma6115258.
[23] Ganesh BKC, Ramanaih N, Chandrasekhar Rao PV. Dry sliding wear behavior of Ti–6Al–4V implant alloy subjected to various surface treatments. Trans Indian Inst Met 2012;65:425–34. https://doi.org/10.1007/s12666-012-0147-4.
[24] Goodman SB. Wear particles, periprosthetic osteolysis and the immune system. Biomaterials 2007;28:5044–8. https://doi.org/10.1016/j.biomaterials.2007.06.035.
[25] Geetha M, Singh AK, Asokamani R, Gogia AK. Ti based biomaterials, the ultimate choice for orthopaedic implants - a review. Prog Mater Sci 2009;54:397–425. https://doi.org/10.1016/j.pmatsci.2008.06.004.
[26] Bartolomeu F, Costa MM, Gomes JR, Alves N, Abreu CS, Silva FS, et al. Implant surface design for improved implant stability – a study on Ti6Al4V dense and cellular structures produced by Selective Laser Melting. Tribol Int 2018. https://doi.org/10.1016/j.triboint.2018.08.012.
[27] Chen Q, Thouas GA. Metallic implant biomaterials. Mater Sci Eng R Rep 2015;87:1–57. https://doi.org/10.1016/j.mser.2014.10.001.
[28] Bauer S, Schmuki P, von der Mark K, Park J. Engineering biocompatible implant surfaces. Part I: materials and surfaces. Prog Mater Sci 2012;58:261–326. https://doi.org/10.1016/j.pmatsci.2012.09.001.
[29] Runa MJ, Mathew MT, Rocha LA. Tribocorrosion response of the Ti6Al4V alloys commonly used in femoral stems. Tribol Int 2013;68:85–93. https://doi.org/10.1016/j.triboint.2013.09.022.
[30] Chen SY, Huang JC, Pan CT, Lin CH, Yang TL, Huang YS, et al. Microstructure and mechanical properties of open-cell porous Ti-6Al- 4V fabricated by selective laser melting vol. 713. 2017. p. 248–54. https://doi.org/10.1016/j.jallcom.2017.04.190.
[31] Fousová M, Vojt D, Jablonská E, Fojt J. Promising characteristics of gradient porosity Ti-6Al-4V alloy prepared by SLM process. J Mech Behav Biomed Mater 2017;69:368–76. https://doi.org/10.1016/j.jmbbm.2017.01.043.
[32] Bose S, Ke D, Sahasrabudhe H, Bandyopadhyay A. Progress in materials science additive manufacturing of biomaterials. Prog Mater Sci 2018;93:45–111. https://doi.org/10.1016/j.pmatsci.2017.08.003.
[33] Wang X, Xu S, Zhou S, Xu W, Leary M, Choong P, et al. Topological design and additive manufacturing of porous metals for bone scaffolds and orthopaedic implants: a review. Biomaterials 2016;83:127–41. https://doi.org/10.1016/j.biomaterials.2016.01.012.
[34] Fazel M, Salimijazi HR, Golozar MA, Garsivaz Jazi MR. A comparison of corrosion, tribocorrosion and electrochemical impedance properties of pure Ti and Ti6Al4V alloy treated by micro-arc oxidation process. Appl Surf Sci 2015;324:751–6. https://doi.org/10.1016/j.apsusc.2014.11.030.
[35] Obadele BA, Andrews A, Mathew MT, Olubambi PA, Pityana S. Improving the tribocorrosion resistance of Ti6Al4V surface by laser surface cladding with TiNiZrO_2 composite coating. Appl Surf Sci 2015;345:99–108. https://doi.org/10.1016/j.apsusc.2015.03.152.
[36] Buciumeanu M, Araujo A, Carvalho O, Miranda G, Souza JCM, Silva FS, et al. Study of the tribocorrosion behaviour of Ti6Al4V – HA biocomposites. Tribol Int 2017;107:77–84. https://doi.org/10.1016/j.triboint.2016.11.029.
[37] Sampaio M, Buciumeanu M, Askari E, Flores P, Souza JCM, Gomes JR, et al. Effects of poly-ether-ether ketone (PEEK) veneer thickness on the reciprocating friction and wear behavior of PEEK/Ti6Al4V structures in artificial saliva. Wear 2016;368–369:84–91. https://doi.org/10.1016/j.wear.2016.09.009.
[38] Cowie RM, Briscoe A, Fisher J, Jennings LM. Wear and friction of UHMWPE-on-PEEK OPTIMA™. J Mech Behav Biomed Mater 2019;89:65–71. https://doi.org/10.1016/j.jmbbm.2018.09.021.
[39] Bartolomeu F, Buciumeanu M, Costa MM, Gasik M, Silva FS, Miranda G. Multi-material Ti6Al4V & PEEK cellular structures produced by Selective Laser Melting and Hot Pressing: a tribocorrosion study targeting orthopedic applications. J Mech Behav Biomed Mater 2018. https://doi.org/10.1016/j.jmbbm.2018.09.009.
[40] Stratton-Powell AA, Pasko KM, Brockett CL, Tipper JL. The biologic response to polyetheretherketone (PEEK) wear particles in total joint replacement: a systematic review. Clin Orthop Relat Res 2016;474:2394–404. https://doi.org/10.1007/s11999-016-4976-z.
[41] Wittenberg RH, Steffen R, Windhagen H, Bücking P, Wilcke A. Five-year results of a cementless short-hip-stem prosthesis. Orthop Rev (Pavia) 2013;5:e4. https://doi.org/10.4081/or.2013.e4.
[42] Moura CG, Pereira R, Buciumeanu M, Carvalho O, Bartolomeu F, Nascimento R, Silva FS. Effect of laser surface texturing on primary stability and surface properties of zirconia implants. Ceram Int 2017;43:15227–36https://doi.org/10.1016/j.ceramint.2017.08.058.
[43] Bagheri ZS, Melancon D, Liu L, Johnston RB, Pasini D. Compensation strategy to reduce geometry and mechanics mismatches in porous biomaterials built with Selective Laser Melting. J Mech Behav Biomed Mater 2017;70:17–27. https://doi.org/10.1016/j.jmbbm.2016.04.041.
[44] Buser D, Janner SFM, Wittneben JG, Brägger U, Ramseier CA, Salvi GE. 10-Year survival and success rates of 511 titanium implants with a sandblasted and acid-etched surface: a retrospective study in 303 partially edentulous patients. Clin Implant Dent Relat Res 2012;14:839–51. https://doi.org/10.1111/j.1708-8208.2012.00456.x.
[45] Fischer K, Stenberg T. Prospective 10-year cohort study based on a randomized controlled trial (RCT) on prostheses . Part 1 : sandblasted and acid-etched implants and mucosal tissue. Clin Implant Dent Relat Res 2012;14:1–8. https://doi.org/10.1111/j.1708-8208.2011.00389.x.
[46] Shunmugavel M, Polishetty A, Littlefair G. Microstructure and mechanical properties of wrought and additive manufactured Ti-6Al-4V cylindrical bars. Procedia Technol 2015;20:231–6. https://doi.org/10.1016/j.protcy.2015.07.037.
[47] Raju R, Duraiselvam M, Petley V, Verma S, Rajendran R. Microstructural and mechanical characterization of Ti6Al4V refurbished parts obtained by laser metal deposition. Mater Sci Eng, A 2015;643:64–71. https://doi.org/10.1016/j.msea.2015.07.029.
[48] Jovanović MT, Tadić S, Zec S, Mišković Z, Bobić I. The effect of annealing temperatures and cooling rates on microstructure and mechanical properties of investment cast Ti-6Al-4V alloy. Mater Des 2006;27:192–9. https://doi.org/10.1016/j.matdes.2004.10.017.
[49] Toh W, Wang P, Tan X, Nai M, Liu E, Tor S. Microstructure and wear properties of electron beam melted Ti-6Al-4V parts: a comparison study against as-cast form. Metals (Basel) 2016;6:284. https://doi.org/10.3390/met6110284.
[50] Koike H, Kida K, Santos EC, Rozwadowska J, Kashima Y, Kanemasu K. Tribology International Self-lubrication of PEEK polymer bearings in rolling contact fatigue under radial loads. Tribiology Int 2012;49:30–8. https://doi.org/10.1016/j.triboint.2011.12.005.
[51] Fellah M, Laba M, Assala O, Dekhil L, Taleb A, Rezag H, et al. Tribological behavior of Ti-6Al-4V and Ti-6Al-7Nb alloys for total hip prosthesis 2014. 2014.